

# Solving Blind Inverse Problems: Adaptive Diffusion Models for Motion-Corrected Sparse-View 4DCT

---

Antoine De Paepe<sup>1</sup>   Alexandre Bousse<sup>1</sup>   Clémentine Phung-Ngoc<sup>1</sup>   Dimitris Visvikis<sup>1</sup>

<sup>1</sup>University of Western Brittany, LaTIM, UMR Inserm 1101, 29238 Brest, France

Fully 3D 2025, Shanghai, China - May 27, 2025



# **Introduction**

---

# Introduction to Lung CT

- **Lung CT Reconstruction:** The reconstruction of lung CT images can be formulated as the following optimization problem:

$$\min_{\mathbf{x}} \frac{1}{2} \|\mathcal{R}\mathbf{x} - \mathbf{b}\|_W^2 + \mathcal{R}(\mathbf{x})$$

# Introduction to Lung CT

- **Lung CT Reconstruction:** The reconstruction of lung CT images can be formulated as the following optimization problem:

$$\min_{\mathbf{x}} \frac{1}{2} \|\mathcal{R}\mathbf{x} - \mathbf{b}\|_W^2 + \mathcal{R}(\mathbf{x})$$

- **Limitations of Static CT:**

- Assumes the patient remains stationary during the scan.
- Respiratory motion can introduce artifacts and blurring.

# Introduction to Lung CT

- **Lung CT Reconstruction:** The reconstruction of lung CT images can be formulated as the following optimization problem:

$$\min_{\mathbf{x}} \frac{1}{2} \|\mathcal{R}\mathbf{x} - \mathbf{b}\|_W^2 + \mathbf{R}(\mathbf{x})$$

- **Limitations of Static CT:**

- Assumes the patient remains stationary during the scan.
- Respiratory motion can introduce artifacts and blurring.

- **Introduction to 4DCT:**

- Captures 3D images across respiratory phases, enabling dynamic lung motion visualization.
- Essential for applications like radiotherapy planning [1].

# Introduction to Dynamic Lung CT

---

- **4DCT Acquisition Modes:**

- Helical mode: The scanner rotates continuously as the patient table moves through the gantry.
- Cine mode: The scanner acquires multiple images at the same table position over a period.
- Uses a surrogate signal (e.g., respiratory belt or external marker) to track breathing motion.

# Introduction to Dynamic Lung CT

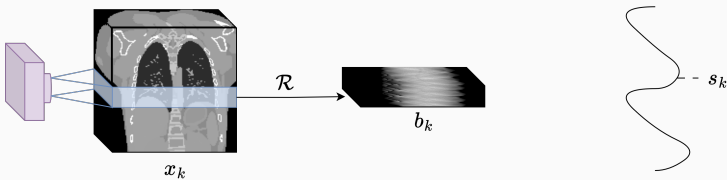
- **4DCT Acquisition Modes:**
  - Helical mode: The scanner rotates continuously as the patient table moves through the gantry.
  - Cine mode: The scanner acquires multiple images at the same table position over a period.
  - Uses a surrogate signal (e.g., respiratory belt or external marker) to track breathing motion.
- **Example of Helical 4DCT Acquisition:**

# Introduction to Dynamic Lung CT

- **4DCT Acquisition Modes:**

- Helical mode: The scanner rotates continuously as the patient table moves through the gantry.
- Cine mode: The scanner acquires multiple images at the same table position over a period.
- Uses a surrogate signal (e.g., respiratory belt or external marker) to track breathing motion.

- **Example of Helical 4DCT Acquisition:**

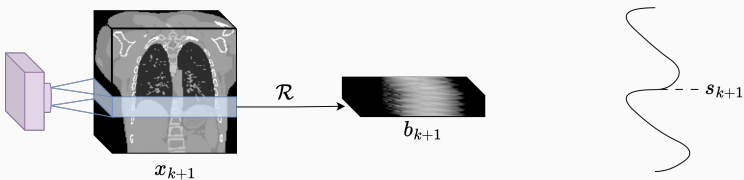


# Introduction to Dynamic Lung CT

- **4DCT Acquisition Modes:**

- Helical mode: The scanner rotates continuously as the patient table moves through the gantry.
- Cine mode: The scanner acquires multiple images at the same table position over a period.
- Uses a surrogate signal (e.g., respiratory belt or external marker) to track breathing motion.

- **Example of Helical 4DCT Acquisition:**

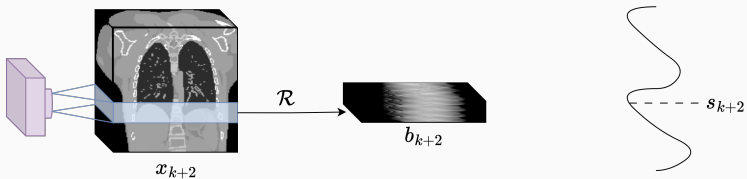


# Introduction to Dynamic Lung CT

- **4DCT Acquisition Modes:**

- Helical mode: The scanner rotates continuously as the patient table moves through the gantry.
- Cine mode: The scanner acquires multiple images at the same table position over a period.
- Uses a surrogate signal (e.g., respiratory belt or external marker) to track breathing motion.

- **Example of Helical 4DCT Acquisition:**

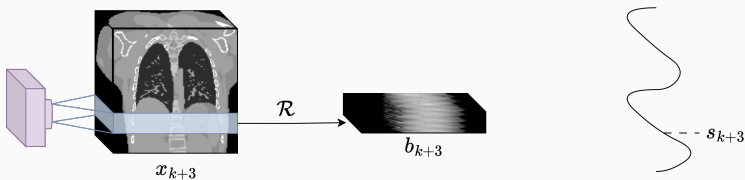


# Introduction to Dynamic Lung CT

- **4DCT Acquisition Modes:**

- Helical mode: The scanner rotates continuously as the patient table moves through the gantry.
- Cine mode: The scanner acquires multiple images at the same table position over a period.
- Uses a surrogate signal (e.g., respiratory belt or external marker) to track breathing motion.

- **Example of Helical 4DCT Acquisition:**



# Challenges in 4DCT

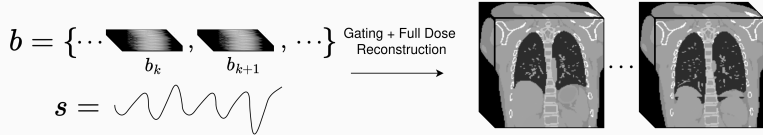
$$b = \{\dots, \overbrace{\phantom{b_k}}, \overbrace{\phantom{b_{k+1}}}, \dots\}$$

$$s = \overbrace{\phantom{s}}$$

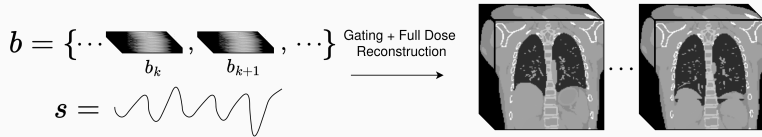
# Challenges in 4DCT

$$b = \{\dots, b_k, b_{k+1}, \dots\} \xrightarrow{\text{Gating + Full Dose Reconstruction}} s = \text{wavy line}$$

# Challenges in 4DCT



# Challenges in 4DCT



- **Challenges:**

- Motion artifacts due to irregular breathing patterns.
- Surrogate signals may not always be stored.
- Increased radiation dose from multiple phase acquisitions; necessitates dose reduction strategies.

# Joint Reconstruction & Motion Estimation (JRM)

- General JRM Framework:

$$\min_{\boldsymbol{x}, \varphi} \frac{1}{2} \|\mathcal{A}_{\varphi} \boldsymbol{x} - \boldsymbol{b}\|_W^2 + \boldsymbol{R}(\boldsymbol{x})$$

where  $\varphi$  are motion parameters.

# Joint Reconstruction & Motion Estimation (JRM)

- General JRM Framework:

$$\min_{\mathbf{x}, \varphi} \frac{1}{2} \|\mathcal{A}_\varphi \mathbf{x} - \mathbf{b}\|_W^2 + \mathbf{R}(\mathbf{x})$$

where  $\varphi$  are motion parameters.

- 4DCT JRM Framework [2]:

$$\min_{\mathbf{x}, \phi, s} \frac{1}{2} \sum_{k=1}^{n_t} \|\mathcal{R} \circ \mathcal{T}_k \circ \mathcal{W}_{\phi \cdot s_k} \mathbf{x} - \mathbf{b}_k\|_W^2 + \mathbf{R}(\mathbf{x})$$

where  $\phi, s$  are deformation vector fields parametrized by B-spline grid and surrogate signals.

# Joint Reconstruction & Motion Estimation (JRM)

- General JRM Framework:

$$\min_{\mathbf{x}, \boldsymbol{\varphi}} \frac{1}{2} \|\mathcal{A}_{\boldsymbol{\varphi}} \mathbf{x} - \mathbf{b}\|_W^2 + \mathcal{R}(\mathbf{x})$$

where  $\boldsymbol{\varphi}$  are motion parameters.

- 4DCT JRM Framework [2]:

$$\min_{\mathbf{x}, \boldsymbol{\phi}, \mathbf{s}} \frac{1}{2} \sum_{k=1}^{n_t} \|\mathcal{R} \circ \mathcal{T}_k \circ \mathcal{W}_{\boldsymbol{\phi} \cdot \mathbf{s}_k} \mathbf{x} - \mathbf{b}_k\|_W^2 + \mathcal{R}(\mathbf{x})$$



where  $\boldsymbol{\phi}, \mathbf{s}$  are deformation vector fields parametrized by B-spline grid and surrogate signals.

# Joint Reconstruction & Motion Estimation (JRM)

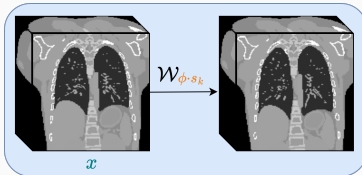
- General JRM Framework:

$$\min_{\mathbf{x}, \varphi} \frac{1}{2} \|\mathcal{A}_\varphi \mathbf{x} - \mathbf{b}\|_W^2 + \mathcal{R}(\mathbf{x})$$

where  $\varphi$  are motion parameters.

- 4DCT JRM Framework [2]:

$$\min_{\mathbf{x}, \boldsymbol{\phi}, \mathbf{s}} \frac{1}{2} \sum_{k=1}^{n_t} \|\mathcal{R} \circ \mathcal{T}_k \circ \mathcal{W}_{\boldsymbol{\phi} \cdot \mathbf{s}_k} \mathbf{x} - \mathbf{b}_k\|_W^2 + \mathcal{R}(\mathbf{x})$$



where  $\boldsymbol{\phi}, \mathbf{s}$  are deformation vector fields parametrized by B-spline grid and surrogate signals.

# Joint Reconstruction & Motion Estimation (JRM)

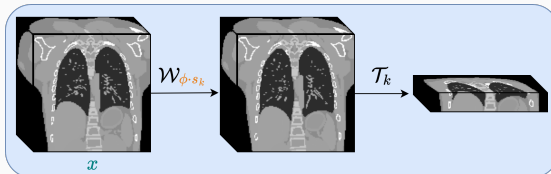
- General JRM Framework:

$$\min_{\mathbf{x}, \boldsymbol{\varphi}} \frac{1}{2} \|\mathcal{A}_{\boldsymbol{\varphi}} \mathbf{x} - \mathbf{b}\|_W^2 + \mathcal{R}(\mathbf{x})$$

where  $\boldsymbol{\varphi}$  are motion parameters.

- 4DCT JRM Framework [2]:

$$\min_{\mathbf{x}, \boldsymbol{\phi}, \mathbf{s}} \frac{1}{2} \sum_{k=1}^{n_t} \|\mathcal{R} \circ \mathcal{T}_k \circ \mathcal{W}_{\boldsymbol{\phi} \cdot \mathbf{s}_k} \mathbf{x} - \mathbf{b}_k\|_W^2 + \mathcal{R}(\mathbf{x})$$



where  $\boldsymbol{\phi}, \mathbf{s}$  are deformation vector fields parametrized by B-spline grid and surrogate signals.

# Joint Reconstruction & Motion Estimation (JRM)

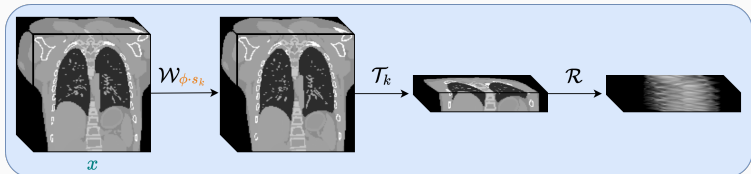
- General JRM Framework:

$$\min_{\mathbf{x}, \boldsymbol{\varphi}} \frac{1}{2} \|\mathcal{A}_{\boldsymbol{\varphi}} \mathbf{x} - \mathbf{b}\|_W^2 + \mathcal{R}(\mathbf{x})$$

where  $\boldsymbol{\varphi}$  are motion parameters.

- 4DCT JRM Framework [2]:

$$\min_{\mathbf{x}, \boldsymbol{\phi}, \mathbf{s}} \frac{1}{2} \sum_{k=1}^{n_t} \|\mathcal{R} \circ \mathcal{T}_k \circ \mathcal{W}_{\boldsymbol{\phi} \cdot \mathbf{s}_k} \mathbf{x} - \mathbf{b}_k\|_W^2 + \mathcal{R}(\mathbf{x})$$



where  $\boldsymbol{\phi}, \mathbf{s}$  are deformation vector fields parametrized by B-spline grid and surrogate signals.

## Methods

---

# Challenges and Proposed Solution

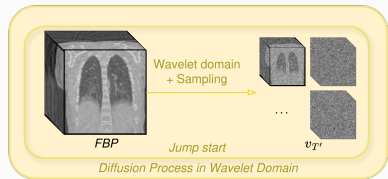
---

- **Challenges:**
  - Sparse-view data increases the ill-posedness of the problem.
  - Hand-crafted regularizers (e.g., Total Variation) tend to oversmooth and erase subtle image features.

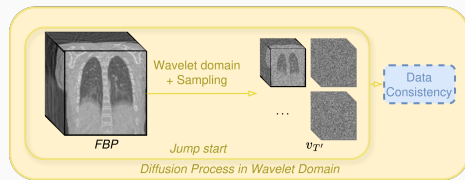
# Challenges and Proposed Solution

- **Challenges:**
  - Sparse-view data increases the ill-posedness of the problem.
  - Hand-crafted regularizers (e.g., Total Variation) tend to oversmooth and erase subtle image features.
- **Solution Overview:**
  - JRM via Adaptive Diffusion Models (ADMs).
  - Motion-free  $\mathbf{x}$  is estimated via a Deep Posterior Sampling (DPS) approach [3].
  - Motion parameters  $\phi, \mathbf{s}$  are estimated through a classical optimization pipeline.
  - Wavelet Diffusion Models (WDMs) [4] are used to enhance computational efficiency.

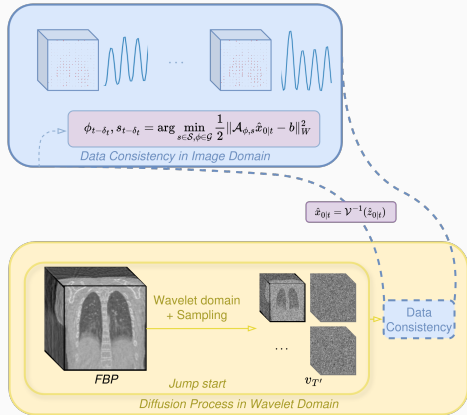
# Overview of JRM-ADM



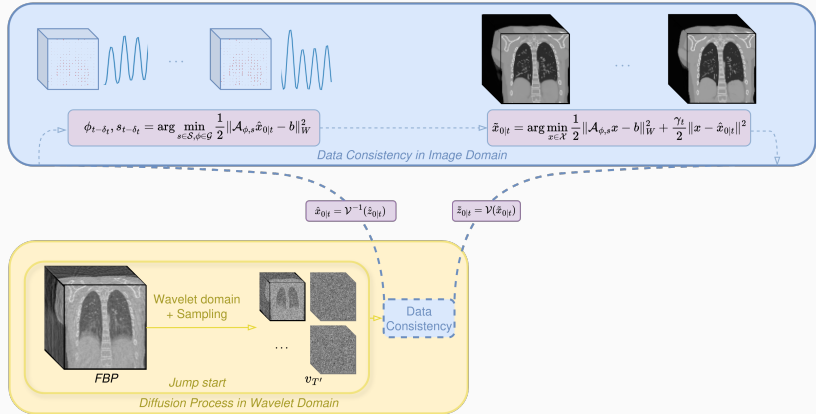
# Overview of JRM-ADM



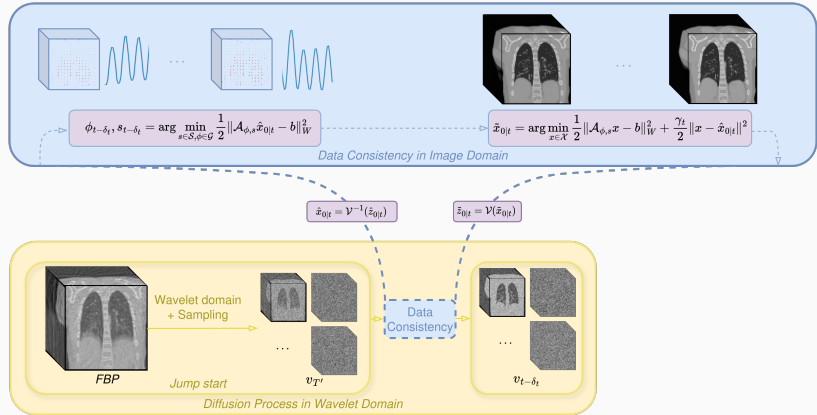
# Overview of JRM-ADM



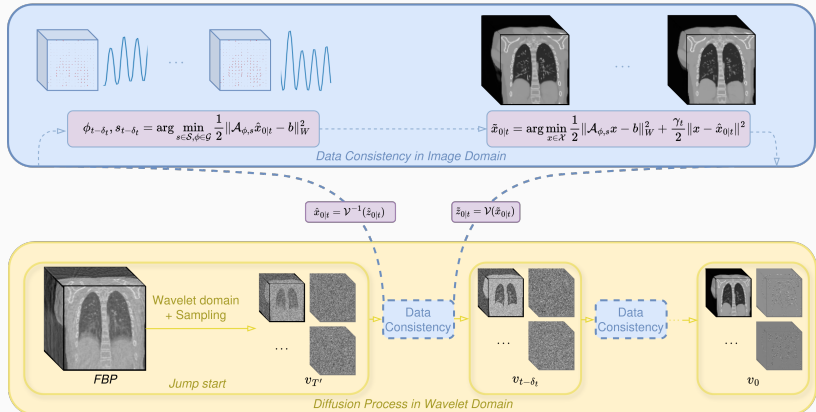
# Overview of JRM-ADM



# Overview of JRM-ADM



# Overview of JRM-ADM



# Experiments

---

# Quantitative Results

---

## Experiments on XCAT

### Phantoms:

- Generated 3D thorax CT volumes ( $128^3$  voxels,  $2.6 \text{ mm}^3$  voxel size) using the XCAT phantoms [5].
- Trained WDMs on these volumes to learn anatomical priors.
- Simulated sparse-view 4DCT acquisitions with 52 projection angles.

# Quantitative Results

## Experiments on XCAT Phantoms:

- Generated 3D thorax CT volumes ( $128^3$  voxels,  $2.6 \text{ mm}^3$  voxel size) using the XCAT phantoms [5].
- Trained WDMs on these volumes to learn anatomical priors.
- Simulated sparse-view 4DCT acquisitions with 52 projection angles.

## Experiments on Pseudo-Real Data:

- Using LIDC-IDRI [6] 3D thorax CT volumes ( $256^3$  voxels,  $1.25 \text{ mm}^3$  voxel size)
- Trained WDMs on these volumes to learn anatomical priors.
- Simulated sparse-view 4DCT acquisitions on CHRU CT volumes with 52 projection angles using a CT respiratory motion synthesis framework [7].

# Quantitative Results

## Experiments on XCAT Phantoms:

- Generated 3D thorax CT volumes ( $128^3$  voxels,  $2.6 \text{ mm}^3$  voxel size) using the XCAT phantoms [5].
- Trained WDMs on these volumes to learn anatomical priors.
- Simulated sparse-view 4DCT acquisitions with 52 projection angles.
- **Evaluation:** Assessed reconstruction quality using metrics such as SSIM and PSNR.

## Experiments on Pseudo-Real Data:

- Using LIDC-IDRI [6] 3D thorax CT volumes ( $256^3$  voxels,  $1.25 \text{ mm}^3$  voxel size)
- Trained WDMs on these volumes to learn anatomical priors.
- Simulated sparse-view 4DCT acquisitions on CHRU CT volumes with 52 projection angles using a CT respiratory motion synthesis framework [7].

# Quantitative Evaluation of Reconstruction Methods

Metric	Gated FBP	Gated DPS	JRM-TV	JRM-ADM
PSNR $\uparrow$	20.59	24.09	25.04	<b>27.05</b>
SSIM $\uparrow$	0.37	0.90	0.89	<b>0.94</b>

**Table 1:** Quantitative evaluation (PSNR, SSIM) of four different reconstruction methods on the end-inhale phase for five XCAT phantoms.

# Qualitative Evaluation of Reconstruction Methods

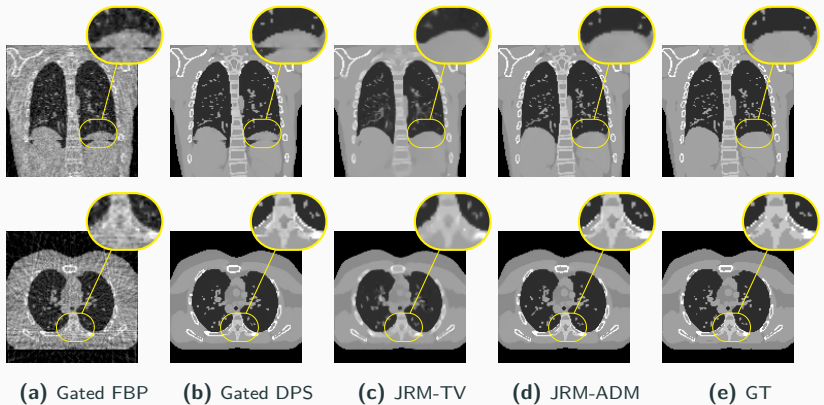


**Figure 1:** GT and end-inhale phase reconstructions on XCAT phantoms.

# Qualitative Evaluation of Reconstruction Methods

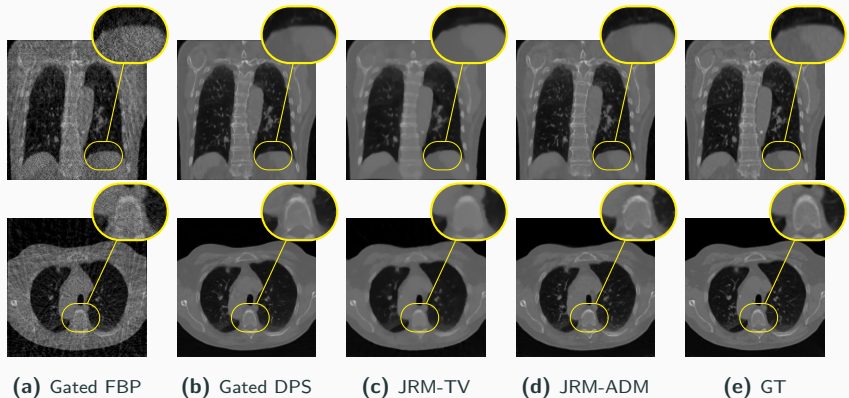


**Figure 2:** GT and reconstructions on pseudo-real data.

# Qualitative Evaluation of Reconstruction Methods

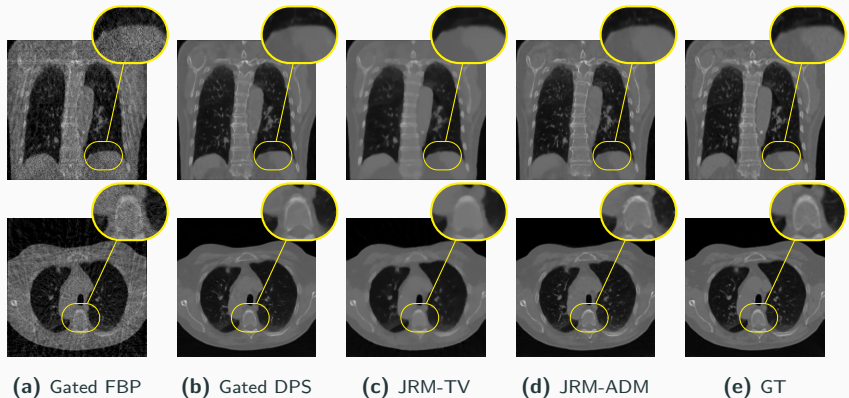


**Figure 2:** GT and reconstructions on pseudo-real data.

# Qualitative Evaluation of Reconstruction Methods

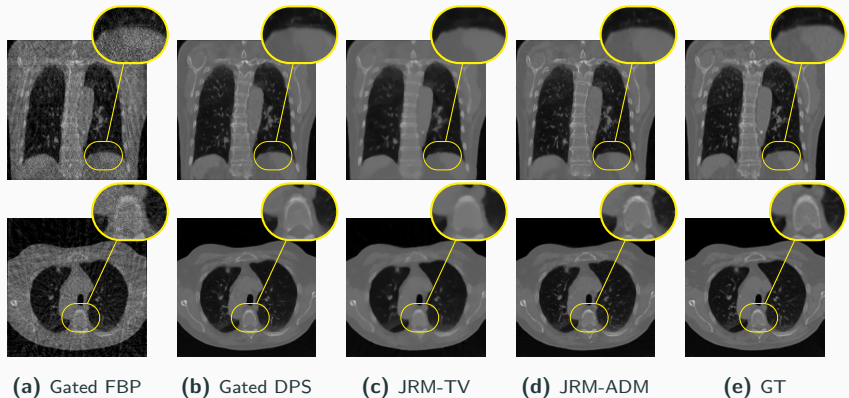


**Figure 2:** GT and reconstructions on pseudo-real data.

# Qualitative Evaluation of Reconstruction Methods

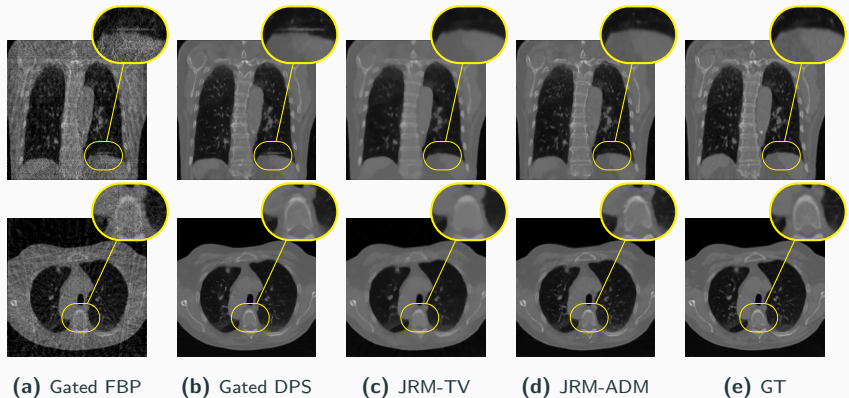


**Figure 2:** GT and reconstructions on pseudo-real data.

# Qualitative Evaluation of Reconstruction Methods

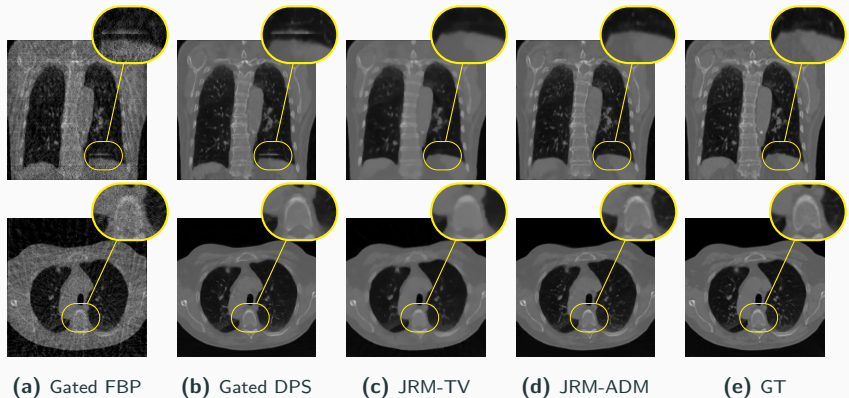


**Figure 2:** GT and reconstructions on pseudo-real data.

# Qualitative Evaluation of Reconstruction Methods

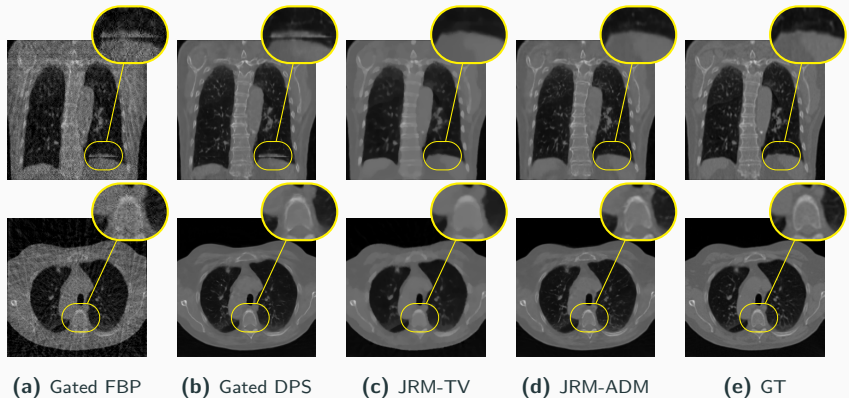


**Figure 2:** GT and reconstructions on pseudo-real data.

# Qualitative Evaluation of Reconstruction Methods

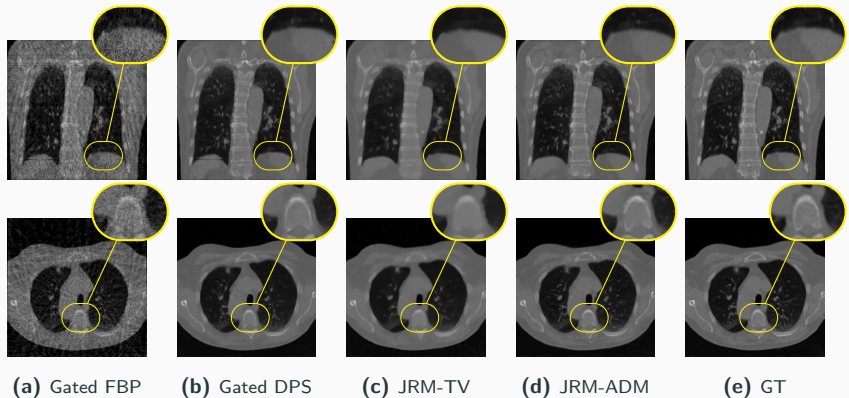


**Figure 2:** GT and reconstructions on pseudo-real data.

# Qualitative Evaluation of Reconstruction Methods

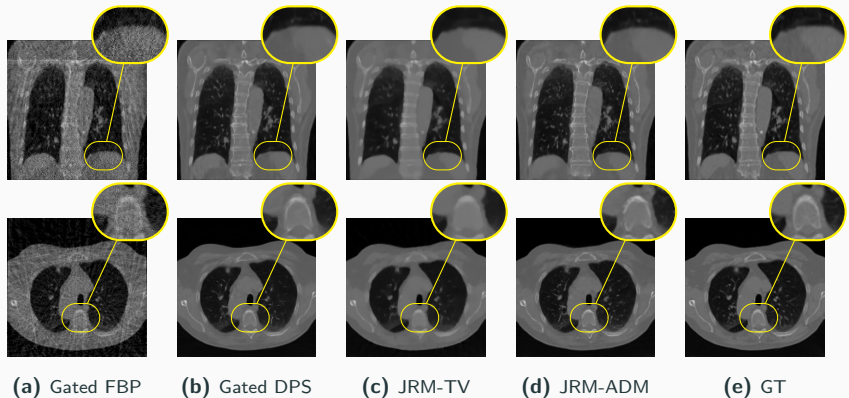


**Figure 2:** GT and reconstructions on pseudo-real data.

# Qualitative Evaluation of Reconstruction Methods

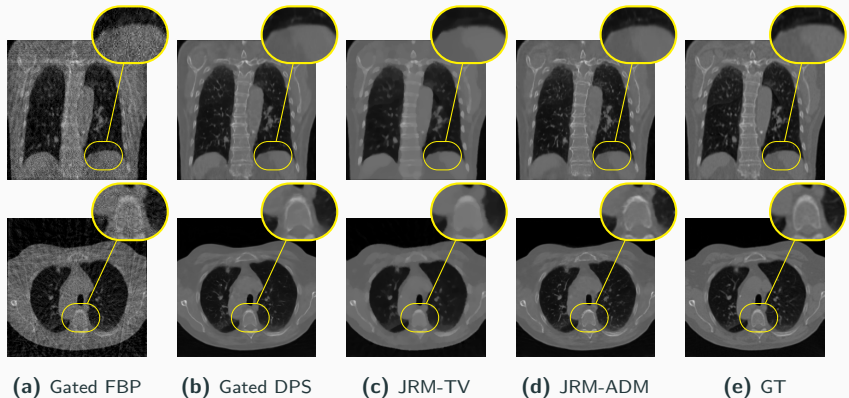


**Figure 2:** GT and reconstructions on pseudo-real data.

# Qualitative Evaluation of Reconstruction Methods

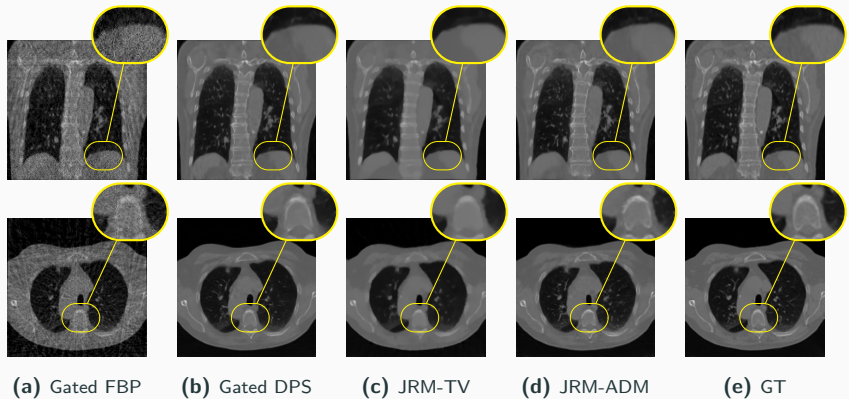


**Figure 2:** GT and reconstructions on pseudo-real data.

# Extension to Motion-Corrected Sparse-View Head CBCT [9]: Quantitative Results

Views	Method	PSNR ( $\uparrow$ )	SSIM ( $\uparrow$ )	MAE $\tau$ ( $\downarrow$ )	MAE $\vartheta$ ( $\downarrow$ )
60	FDK	17.00	0.23	-	-
	JRM-TV	28.91	0.90	0.34	0.11
	JRM-ADM	<b>29.67</b>	<b>0.92</b>	<b>0.27</b>	<b>0.09</b>
40	FDK	16.92	0.19	-	-
	JRM-TV	27.19	0.87	0.43	0.12
	JRM-ADM	<b>28.66</b>	<b>0.91</b>	<b>0.29</b>	<b>0.11</b>
20	FDK	14.96	0.14	-	-
	JRM-TV	23.38	0.75	0.86	0.17
	JRM-ADM	<b>27.18</b>	<b>0.87</b>	<b>0.30</b>	<b>0.12</b>

**Table 2:** Quantitative results of methods in comparison on the CQ500 [8] dataset for the motion corrected reconstruction tasks under sparse-view settings of 60, 40, and 20 views.

# Extension to Motion-Corrected Sparse-View Head CBCT [9]: Qualitative Results

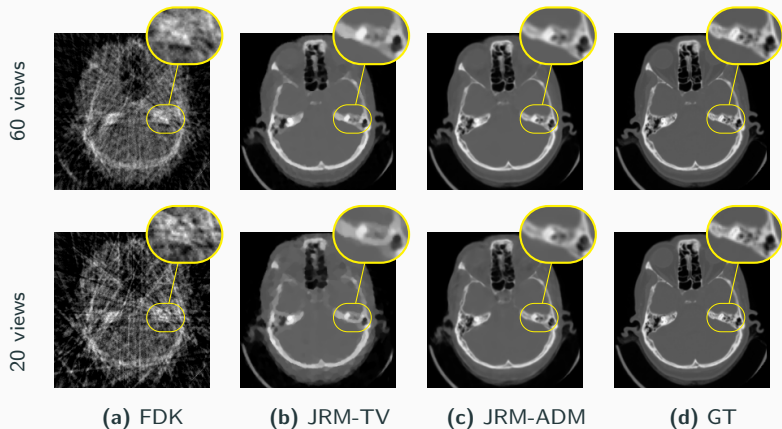


**Figure 3:** GT and reconstructions (axial plane) for motion-affected sparse-view CBCT: results are shown for 40- and 20-view acquisition settings.

## **Conclusion - Discussion**

---

## Conclusion & Discussion

---

- **High-fidelity 4DCT:** JRM-ADM yields artifact-free, high-resolution reconstructions under irregular breathing, outperforming classical reconstruction methods.

## Conclusion & Discussion

---

- **High-fidelity 4DCT:** JRM-ADM yields artifact-free, high-resolution reconstructions under irregular breathing, outperforming classical reconstruction methods.
- **Computational Challenges:** GPU memory and runtime remain high; future work should explore how to solve this.

## Conclusion & Discussion

---

- **High-fidelity 4DCT:** JRM-ADM yields artifact-free, high-resolution reconstructions under irregular breathing, outperforming classical reconstruction methods.
- **Computational Challenges:** GPU memory and runtime remain high; future work should explore how to solve this.
- **Real World Challenges:** Working on real sinograms would be the best path toward clinical translation.

# References i

---

-  Yune Kwong, Alexandra Olimpia Mel, Greg Wheeler, and John M Troupis.  
**Four-dimensional computed tomography (4dct): a review of the current status and applications.**  
*Journal of medical imaging and radiation oncology*, 59(5):545–554, 2015.
-  Yuliang Huang, Bjoern Eiben, Kris Thielemans, and Jamie R McClelland.  
**Resolving variable respiratory motion from unsorted 4d computed tomography.**  
In *International Conference on Medical Image Computing and Computer-Assisted Intervention*, pages 588–597. Springer, 2024.
-  Yuanzhi Zhu, Kai Zhang, Jingyun Liang, Jiezhang Cao, Bihan Wen, Radu Timofte, and Luc Van Gool.  
**Denoising diffusion models for plug-and-play image restoration.**  
In *Proceedings of the IEEE/CVF Conference on Computer Vision and Pattern Recognition*, pages 1219–1229, 2023.
-  Paul Friedrich, Julia Wolleb, Florentin Bieder, Alicia Durrer, and Philippe C Cattin.  
**Wdm: 3d wavelet diffusion models for high-resolution medical image synthesis.**  
In *MICCAI Workshop on Deep Generative Models*, pages 11–21. Springer, 2024.
-  W Paul Segars, G Sturgeon, S Mendonca, Jason Grimes, and Benjamin MW Tsui.  
**4d xcat phantom for multimodality imaging research.**  
*Medical physics*, 37(9):4902–4915, 2010.

## References ii

-  Samuel G Armato III, Geoffrey McLennan, Luc Bidaut, Michael F McNitt-Gray, Charles R Meyer, Anthony P Reeves, Binsheng Zhao, Denise R Aberle, Claudia I Henschke, Eric A Hoffman, et al.  
**The lung image database consortium (lidc) and image database resource initiative (idri): a completed reference database of lung nodules on ct scans.**  
*Medical physics*, 38(2):915–931, 2011.
-  Yi-Heng Cao, Vincent Bourbonne, François Lucia, Ulrike Schick, Julien Bert, Vincent Jaouen, and Dimitris Visvikis.  
**Ct respiratory motion synthesis using joint supervised and adversarial learning.**  
*Physics in Medicine & Biology*, 69(9):095001, 2024.
-  Sasank Chilamkurthy, Rohit Ghosh, Swetha Tanamala, Mustafa Biviji, Norbert G Campeau, Vasantha Kumar Venugopal, Vidur Mahajan, Pooja Rao, and Prashant Warier.  
**Deep learning algorithms for detection of critical findings in head ct scans: a retrospective study.**  
*The Lancet*, 392(10162):2388–2396, 2018.
-  Antoine De Paepe, Alexandre Bousse, Clémentine Phung-Ngoc, Youness Mellak, and Dimitris Visvikis.  
**Adaptive diffusion models for sparse-view motion-corrected head cone-beam ct.**  
*arXiv e-prints*, pages arXiv–2504, 2025.